Stability of the nanomartensitic phase in ultrathin Fe films on Cu(100)

A. Biedermann
Faculty of Physics, University of Vienna, A-1090 Vienna, Austria
(Received 19 October 2009; published 2 December 2009)

The stability of the bcc-like "nanomartensitic" (NM) phase in epitaxial Fe films grown layer by layer on Cu(100) is characterized by variable-temperature scanning tunneling microscopy. While 3 monolayer (ML) films are found to be completely NM at least up to 340 K, films 4 and 5 ML thick are pseudomorphic fcc but show a transition to the NM phase induced by hydrogen adsorption. A statistical mechanical description of these transitions, in particular of the surface H distribution in the region of fcc-NM phase coexistence, is used to estimate the free-energy difference $\Delta F^{\mathrm{fcc}\rightarrow\mathrm{NM}}$ in dependence of thickness and temperature: The continuously increasing stability of the NM phase with decreasing thickness, qualitatively reflected in the decreasing H_2 doses required to stabilize it ($\approx$100 L, $\approx$0.5 L, and none for 5, 4, and 3 ML films), is explained by finite-thickness terms in the energy balance which are detectable already in 5 ML films but can overcome the fcc-stabilizing lattice mismatch terms only in films less than 4 ML thick. Furthermore it is found that the NM phase, like bulk bcc Fe, becomes more stable with decreasing temperature. However, below 200 K the relative stability is almost temperature independent, i.e., phase changes between fcc and NM can still be fully controlled by hydrogen adsorption but hardly by temperature variation. These results are discussed in terms of finite-thickness modifications to current zero-temperature and finite-temperature models of bulk Fe, in particular that by Hasegawa and Pettifor [H. Hasegawa and D. G. Pettifor, Phys. Rev. Lett. **50**, 130 (1983)], which emphasizes the importance of the magnetic free energy for the phase stability of Fe.

DOI: 10.1103/PhysRevB.80.235403 PACS number(s): 64.70.Nd, 68.37.Ef, 75.50.Bb, 81.30.Kf

I. INTRODUCTION

Phase stability and phase transitions are essential for the design of functional materials. In Fe and its alloys one type of functionality is given by the direct relation of crystal structure (fcc, bct, or bcc) and ferromagnetic properties, another by temperature-dependent displacive (ferroelastic) transitions between these phases, giving rise to various magnetoelastic (e.g., magnetic shape memory effect in Fe-Pd alloys[1]) and thermoelastic (e.g., tunable thermal-expansion coefficients in Fe-Ni alloys) functionalities. In recent years it became apparent that similar transitions are relevant also in ultrathin Fe films but in different and unexpected ways. The bulk ground-state structure of Fe is bcc, while the fcc phase is marginally more stable [by less than 1 meV/atom (Ref. 2)] only in a temperature window between 1185 and 1667 K. It is further known that, by virtue of near perfect lattice matching, the Fe fcc phase can be stabilized at low temperatures in films grown on Cu(100) single crystals, as long as they are less than about 11 monolayers (ML) thick.[3,4] Surprisingly, however, there is also a *lower* thickness limit for the stability of the fcc phase: Films less than 5 ML thick form a nanomartensitic (NM) phase[5,6] (Fig. 1) whose distinctly bcc-like character provides a natural explanation for their strong ferromagnetism with Curie temperatures up to 380 K in 3 ML films.[7] However, there is no clear picture yet of what stabilizes the NM phase, provoking fundamental questions regarding the nature of (finite temperature) phase stability in Fe nanostructures with large surface-to-volume ratios. Answering these questions is relevant as even the origin of the phase stability in bulk Fe remains controversial, e.g., whether phonon[8] or magnon[9] contributions to the free energy are more important. Understanding phase stability in nanoscale Fe is particularly relevant for potential applications aiming at the microscopic manipulation of magnetic properties, such as magnetic patterning, exploiting phase changes in ultrathin metastable fcc Fe films by ion irradiation.[10]

The main themes of this paper are the temperature and thickness dependent stability of the NM phase relative to the fcc phase. It turns out that temperature-dependent measurements alone are insufficient as H contamination is difficult to avoid completely even under ultrahigh-vacuum conditions, requiring the introduction of H coverage as an additional parameter. Rather than being an additional complication, however, H adsorption provides a useful additional thermodynamic degree of freedom to probe the phase stability. The fact that surface H plays an important role for the magnetic and structural properties of this system has been shown by Vollmer and Kirschner,[11] who find a correlated increase in the film magnetization and appearance of a film fraction with increased interlayer distance on exposing 4 ML Fe/Cu(100) films to very small H_2 doses.

The NM structure forms by shear deformation of the fcc lattice in alternating directions (cf. Fig. 1),[12] which is accompanied by an increase in the interlayer distance by about 5–6 %.[4,13] This large increase corresponds to a modest decrease in the interatomic distance between Fe atoms in adjacent layers by about 2% from fcc [0.253 nm (Ref. 4)] to bcc (0.248 nm) values.[12] Based on experimental evidence and theoretical predictions it can be assumed that the shear deformation is by and large equal in all Fe layers except the interface monolayer, which is less sheared: Even films only 2 ML thick show at least locally the ideal NM structure in scanning tunneling microscope (STM) images.[12] First-principles calculations[6] of 3 ML films show equal shear angles of the two topmost layers, a significantly less sheared interface Fe layer, and a weakly sheared Cu interface layer.

The NM phase differs from typical bulk Fe martensitic phases by an extremely high density of twin boundaries

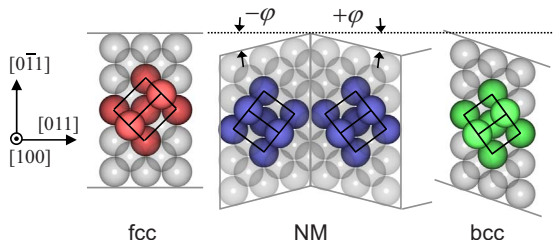

FIG. 1. (Color online) Top view of the nanomartensitic crystal structure in Fe/Cu(100) films in comparison to fcc(100) and bcc(110). The respective body-centered unit cells, seen edge on, are outlined and the atoms constituting them rendered solid while the remaining atoms are rendered transparent. Shown on the left-hand side are the fcc substrate lattice directions. The alternating shear angle $\pm\varphi$ of the ideal NM structure is $\approx 14°$ although structures with inhomogeneous $\varphi \approx 5-15°$ may occur at elevated temperatures (cf. Sec. III A). The shear angle of the ideal bcc structure is 19.5°.

(where the shear angle φ changes its sign), corresponding to a zigzag period of the NM structure of typically $n=6$ atom rows as shown in Fig. 1 with a small variation in $n=4-5$ in 3 ML films (e.g., Fig. 2) and $n=6$ in 4 ML films leading to characteristic $(1\times n)$ fractional-order spots in low-energy electron-diffraction patterns.[4] In the 5-ML NM phase first described in this paper, (cf. Sec. III D) n seems to be even a little higher. This twinning appears to be an interface effect trading off the energy loss due to the extremely high density of boundaries by the considerably lowered Fe-Cu interface energy, since no Fe atom has to be translated too far from its fcc position. Since interface mismatch is relevant only for very thin films, already in 6 ML films variants with the same local structure as the NM phase but with a much lower twin boundary density appear (≥ 8 atom rows between boundaries).[12,14] For a complete description, this direct competitor of the NM and bcc phase is important, but is nevertheless excluded from the scope of this paper.

As a second difference to bulk Fe martensite, the strain in the NM phase in fcc[011] direction (cf. Fig. 1) necessary to match the interrow distance with that of the Cu substrate in that direction is much higher ($\approx 10\%$) (Ref. 15) than the residual strain in typical martensitic Fe phases, where most of the strain due to structural mismatch between fcc and bcc is relieved by forming dislocations at the interfaces. By way of contrast, the NM structure attempts to match both local bcc symmetry and global fcc symmetry simultaneously without introducing such high energy defects, which bears some resemblance to "adaptive" phases in bulk crystals, which are thought to appear as intermediate "microtwinned" phases in bulk phase transitions.[16]

The following sections describe the experimental results for 3 and 4 ML films followed by a separate section dedicated to the statistical thermodynamics of the H induced fcc-NM phase transition in the H/Fe/Cu(100) system, which is most useful for the description of 4 ML films. All results regarding 5 ML films are combined in the subsequent and last results section. In the discussion section, these thickness and temperature-dependent results are generalized with the goal to find correspondences and differences to bulk Fe in order to convey a broader perspective besides the immediate surface science related issues.

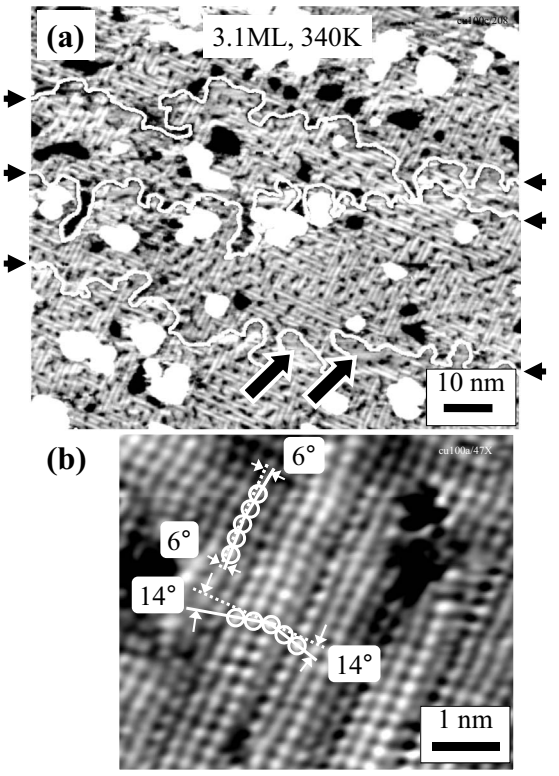

FIG. 2. STM images of 3 ML films at 340 K. (a) Overview image at −10 mV/1 nA sample voltage/current. Terraces separated by monatomic steps (white lines marked by arrows at image border) are brought to same level. The image contrast of this and all other images in this paper is rather high, about 50 p.m. between black and white. Therefore 4 ML islands and 3 ML holes appear completely white and black, respectively. The film is completely nanomartensitic except in small regions at step edges where the film is locally 4 ML thick (large arrows in lower part of image). Each ≈1 nm wide stripe corresponds to a reflection-twin pair typically 4–5 atom rows wide (zigzag period) in the (b) atomically resolved image (−1 mV/5 nA). Local shear angles with respect to fcc⟨110⟩ directions are indicated.

II. EXPERIMENTAL

The experiments were carried out using a variable-temperature STM in an ultrahigh-vacuum (UHV) chamber with a base pressure below 1×10^{-10} mbar. Sample temperatures in the STM were set between 130 and 340 K using a counterheated flow cryostat operated with liquid nitrogen and connected to the sample holder via a cold finger or by a heating element inside the sample holder. The temperature was measured either using a diode thermometer in the cold finger clamping block or by using a resistance thermometer inside the sample holder. In all cases the temperature drop between thermometer and sample was approximately corrected resulting in a temperature accuracy of about 10% of the difference to the STM base temperature of 300 K for temperatures below 300 K and 20% for temperatures above 300 K. Heating and cooling rates were in the range of 1–3 K/min during imaging except noted otherwise, rates for temperature changes over larger temperature intervals without imaging typically 5–10 K/min.

The Cu(100) samples were cleaned by sputtering with 5 keV Ar^+ ions followed by annealing to typically 770 K. The Fe films were grown at 300 K substrate temperature by evaporation from Fe wire heated by electron bombardment with the sample in the STM. The growth rate was typically 0.1–0.3 ML/min. The thickness was checked intermittently by STM with the tip fully withdrawn during deposition.

H dosing was done by increasing the H_2 partial pressure in the entire chamber for a few minutes. The H_2 dose values in this paper are given in Langmuir units, $f \times p \times t$, with ion gauge reading p in units of 10^{-6} torr, dosing time t in seconds, and a correction factor $f=2.5\pm0.5$ for H_2 relative to N_2. To correct for the unavoidable H_2 dosing due to the residual H_2 pressure in the chamber, the H_2 partial pressure was measured by a quadrupole mass spectrometer calibrated using the ion gauge. The uncertainty of the total H_2 dose at the time of measurement is therefore given by the precision of the ion gauge and the uncertainty of f and is estimated to 50%.

III. RESULTS

A. 3 ML films

Three ML films have been imaged with atomic resolution at 80 K in previous works,[5,12] characterizing the groundstate structure in excellent agreement with first-principles calculations.[6] By way of contrast, the 3 ML experiments presented here focus on the finite temperature structure at up to 340 K. At this temperature, H_2 desorption from the NM Fe surface is fast enough to reduce the residual H contamination to a very low level.[11] As shown in Fig. 2(a) the entire film surface shows the nanomartensitic reconstruction. In Fig. 2(a) each "stripe" typ. ten-nm-long and 1–2-nm-wide represents a five-atom-rows-wide NM reflection-twin pair. This type of contrast is mainly due to a slightly increased apparent height of one of the two reflection twins of the NM structure and presumably the consequence of a slightly noncylindrical symmetry of the tunneling tip apex.

The ideal NM shear angle of 14° known from 80 K images of 3 ML films,[5] is seen also in the images at 340 K, but only locally, while the most likely angles in an ensemble of five images such as that in Fig. 2(b) acquired between 300 and 340 K are in the 8–10° range. In particular near boundaries between rotational domains, where a mismatch between zigzag and straight atom rows occurs, the shear angle is distinctly reduced [e.g., upper left quadrant in Fig. 2(b)]. It seems that in regions sufficiently far away from such fcc-stabilizing defects, the ideal NM structure forms even at 340 K. Since, however, the density of rotational domain boundaries is very high [cf. Fig. 2(a)], ideal NM regions are rare, leading to a reduced shear angle on average. This temperature-dependent reduction of the shear angle on average, which should have an effect on the interlayer distance assuming a hard-sphere model, may be compared to an energy dependent low-energy electron-diffraction (LEED I/V, single scattering) analysis by Zharnikov *et al.*[13,17] On raising the temperatures above 200 K, the energy dependent intensity (I/V) curves show an increase in the small signal at the position for the fcc interlayer distance (176 eV) relative to the peak for the increased interlayer distance of the NM phase (145 eV), which is fully reversible. Inspection of the I/V curves[13] at 153 and 343 K shows that this increase in the 176 eV value could be interpreted as a broadening of the 145 eV peak toward higher energies, which is qualitatively expected for incoherent scattering from a structure with a certain variation in the interlayer distance toward smaller values.

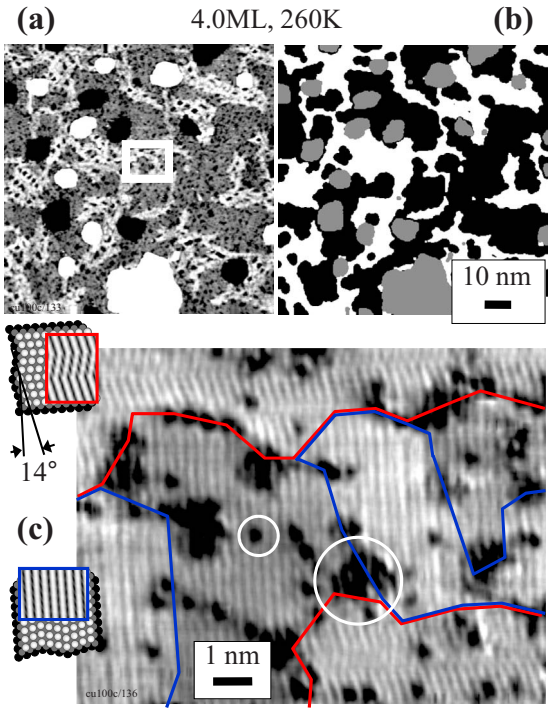

FIG. 3. (Color online) STM images of a mildly annealed (330 K) 4 ML film imaged at 260 K with a residual H surface coverage of a few percent. (a) Overview image (−1 V/1 nA) with high image contrast (cf. caption Fig. 2). The NM phase appears brighter than the fcc phase. (b) Result of a level based segmentation showing NM regions white, fcc regions black, and 3 ML holes and 5 ML islands gray. (c) High resolution detail (−1 mV/5 nA) of the area marked by the rectangle in (a). Vertical stripes are individual atom rows; the atoms in the rows are not resolved due to a diatomic tip. The insets simulate this effect by a near vertical blurring of the schematic surface model shown underneath by one interatomic distance. The two orthogonal domains are outlined. The small black spots are individual O and C atoms (small circle), the larger ones due to embedded Cu (large circle, cf. text).

B. 4 ML films

Four ML Fe films as grown at 300 K are predominantly fcc, but can be partially nanomartensitic depending on the preparation conditions.[12] In this work it is found that the NM fraction strongly increases on reducing the temperature by as little as 40 K (Fig. 3). In this section it will be shown that this somewhat ill-defined transition behavior is caused mainly by two separate "ingredients:" (1) the presence of surface H in the single-digit percent range stabilizing the NM phase and (2) the strongly temperature-dependent stability of this phase.

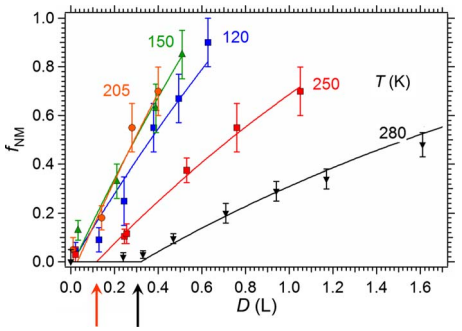

FIG. 4. (Color online) Nanomartensitic fraction in 4 ML films in dependence of H_2 dose at different temperatures. Lines are curve fits based on the statistical mechanical model (Sec. III C). The 250 and 280 K curves show significant temperature-dependent onset delays (arrows).

In contrast to 3 ML films, the average shear angle of the 4-ML NM phase is quite close to 14° [see Fig. 3(c) and Ref. 12] even at 300 K. The fraction of the film that is nanomartensitic f_{NM} is quantified by an image segmentation algorithm based on the different apparent heights of the NM and fcc phases due to their different interlayer distances as exemplified in Fig. 3(b). The NM phase always shows a small density of dark spots [large circle in Fig. 3(c)], which are a few times larger than the apparent size of individual surface impurity atoms. These are small fcc regions forming preferentially near small islands of embedded Cu and can show an increased density of the residual C and O contamination atoms (typ. ≈5% coverage averaged over entire film surface), which tend to avoid the NM phase. The segmentation algorithm includes these islands in the NM film fraction to make it more robust with respect to variations in image quality. Monolayer holes and islands are excluded, i.e., $f_{NM}=1$ if all 4 ML parts of the film are NM irrespective of the structure of 3 ML holes (always NM) and 5 ML islands (fcc or NM).

To completely desorb any residual H, the films were heated to or slightly above 350 K. The minimum annealing temperature and time is given by the requirement that the NM fraction is less than 10% after cooling to 150 K indicating a H coverage of less than about 1%. Above 350 K the formation of small holes[18] in the films starts, which initiate the transformation toward more three-dimensional-like Fe films covered by Cu, and care has to be taken to keep their density low (typically less than a few holes per μm^2). Note that the formation of these holes at low temperatures does not imply significant Cu diffusion to the surface, which requires higher temperatures to become efficient[19] and can be checked directly by STM exploiting the distinct image contrast between Cu and Fe.[12]

Subsequently, the NM fraction f_{NM} was determined in dependence of H_2 dose D and temperature T by performing constant-temperature dosing experiments $f_{NM}(D)|_T$ (Fig. 4). The shape of these curves is very linear, which will be relevant for the atomistic description of the transition process in the next section. Most notably, their average slope is very temperature dependent above 200 K but almost temperature independent below. The curves also match the increase in the film magnetization in dependence of H_2 dose seen by Vollmer and Kirschner,[11] showing that the NM phase is the origin of the film magnetization responsible for Curie temperatures above 300 K.[7]

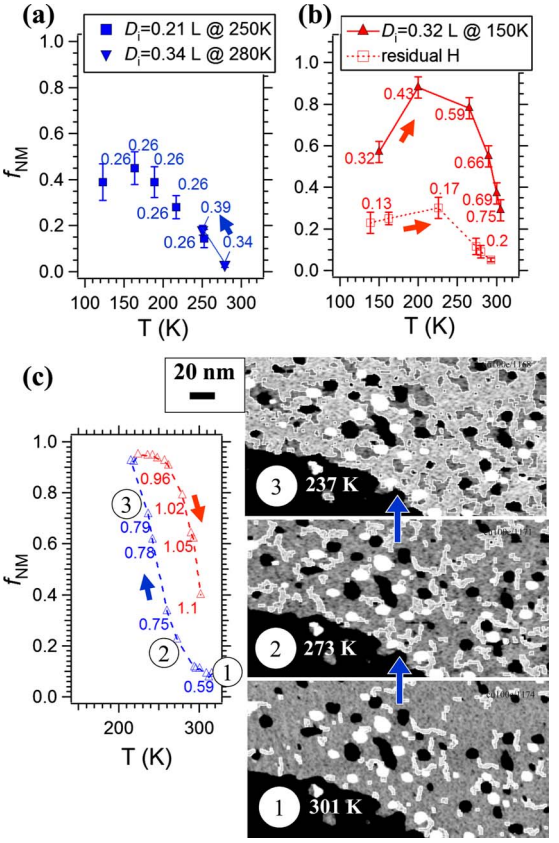

FIG. 5. (Color online) Nanomartensitic fraction in 4 ML films in dependence of temperature. The actual H_2 dose D for each individual point indicated in the graphs is the initial dose D_i increased by the unavoidable H_2 dose due to the residual H_2 partial pressure. Lines indicate sequential measurements with the direction indicated by arrows. (a) Dosing 0.21 L at 250 K or 0.34 L at 280 K, respectively, on well annealed films (cf. text) and cooling to the respective measurement temperature. (b) Starting at low temperatures with a certain initial H_2 dose, the films are heated, stopping before significant H_2 desorption starts. Heating rate of the lower curve is higher than normal (5–10 K/min, cf. Sec. II) minimizing background H_2 adsorption. (c) Temperature cycle starting just below 320 K. Three STM images of the sequence illustrate the rapidly increasing NM fraction on cooling (−1 V, 0.1 nA, bright NM areas are outlined by white lines).

To rule out a temperature-dependent sticking coefficient, which could result in similar temperature dependence, also constant-coverage experiments $f_{NM}(T)|_{\Theta_H}$ were performed. In the first type of experiment, each cycle is started by adsorbing hydrogen on the annealed film at a fixed temperature T_0 (e.g., 250 K) prior to cooling to the measurement temperature T to determine $f_{NM}(T)$ [Fig. 5(a)]. Each cycle is finished by annealing again to prepare for the next measurement with the same T_0 but different T. This rather tedious procedure guarantees that the effective H coverage Θ_H for each measurement point is equal, even if the sticking coefficient depends on temperature and residual H_2 adsorbs during cooling down to T. However, no significant inconsistencies

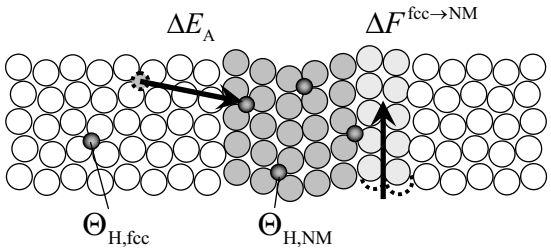

FIG. 6. Schematic top view of Fe films with coexisting H-induced NM phase and (2×2)p4g surface reconstructed fcc phase.[15] The two arrows symbolize the processes associated to the two energy parameters ΔE_A and $\Delta F^{fcc\rightarrow NM}$ of the statistical mechanical model. ΔE_A is the gain in adsorption energy if one H atom is transferred from an fcc site to a NM site. $\Delta F^{fcc\rightarrow NM}$ is the average free energy per Fe atom necessary to change the fcc phase to the NM phase. The number of H atoms shown approximately represent to the local H coverages $\Theta_{H,fcc}$ and $\Theta_{H,NM}$ on a 4 ML film at 200 K [cf. Fig. 7(b)].

between constant-coverage and constant-temperature experiments (Fig. 4) have been found. In a second group of experiments, a film exposed to a defined dose at 150 K and a film with a small residual H coverage (from incomplete annealing) starting at 130 K were heated to probe the reverse transition [Fig. 5(b)]. These curves necessarily suffer from unwanted adsorption of residual H_2 gas in the chamber, i.e., are not exactly at constant coverage. Nevertheless, comparison with the cooling curves in Fig. 5(a) reveals a significant hysteresis, i.e., the reverse transition NM→fcc takes place about 50 K higher. Note that the phase transition, i.e., the decrease in the NM fraction on heating between 250 and 300 K is not related to H_2 desorption, which becomes relevant on the time scale of the experiment only above 300 K. This can be directly seen in the temperature cycle experiment at rather large H coverage starting in the state of desorbing H_2 [Fig. 5(c)]. In the initial phase the film was heated until the NM fraction decreases slowly due to H_2 desorption, which occurs close to 320 K. On cooling, the NM fraction immediately stopped to decrease and started to increase at a high rate below 300 K. Of course, in this case (and for the film with residual H coverage) the initial dose is only approximately known and is determined *a posteriori* in the course of the quantification procedure in the next section.

C. Statistical thermodynamics of 4 ML H/Fe/Cu(100) films

Clearly, the H coverage Θ_H correlates with the NM fraction f_{NM}, but how is this exact correlation maintained? The weakly convex shape of the $f_{NM}(D)$ curves (Fig. 4) shows that hydrogen does not adsorb predominantly on the NM phase, which would result in a distinctly concave shape. This implies that after dissociative adsorption, the hydrogen atoms must diffuse to the NM regions of the film to promote their growth, held there by a small adsorption energy difference ΔE_A (Fig. 6). In every two-level system the population of the lower energy level (adsorption sites on NM phase) drops with increasing temperature while the population of the higher energy level (adsorption sites on the fcc phase) is raised. Since there must be a minimum H coverage on the NM phase to stabilize it, a temperature-dependent threshold dose must and does exist (onset delays in the 250 and 280 K curves in Fig. 4) which provides a measure of the energy difference ΔE_A.

The phase stability is now quantified by determining the average Helmholtz free-energy difference $\Delta F^{fcc\rightarrow NM}$ per Fe atom between the fcc and NM phase from the observed $f_{NM}(D)$ and $f_{NM}(T)$ curves. To describe the system, an augmented version of the classic Langmuir-McLean segregation model[20] is used. Segregation usually deals with impurity atoms coming from the bulk and segregating on a fixed number of attracting surface sites. Here, H atoms coming from a variable number of fcc surface sites s_f segregate on a variable number of attracting NM surface sites s_b. The increase in s_b by the fcc-NM phase transition increases the film energy by $d\Delta F^{fcc\rightarrow NM}$ with the film thickness d in ML. Therefore the total energy ε relative to an fcc film with the same number of H atoms on it may be approximated as

$$\varepsilon \approx n_b \Delta E_A + s_b d \Delta F^{fcc\rightarrow NM}(T,d) \tag{1}$$

with the number of H atoms on the NM and fcc fraction, n_b and n_f, respectively. H atom and adsorption site numbers are constrained by the conservation relations for the total H atom number n and the total surface Fe atom number s,

$$s = s_b + 2s_f, \quad n = n_b + n_f. \tag{2}$$

Factor 2 is due to the assumption that H atoms occupy predominantly rhomblike sites of the reconstructed fcc surface,[15] which are very similar to the adsorption sites on the NM phase (cf. Fig. 6).

The equilibrium configuration, i.e., the H atom number on the NM phase n_b and the NM adsorption sites s_b minimizing the H configuration related free energy, is determined by finding the maximum term of the lattice partition function for noninteracting H atoms with the degeneracies, i.e., the number of possible H configurations for fixed s_b and n_b written as binomial coefficients

$$Z = \sum_{s_b} \sum_{n_b} \binom{s_f}{n_f} \binom{s_b}{n_b} e^{-\varepsilon(n_b,s_b,T,d)/k_B T} \tag{3}$$

To determine the free energy of the entire system, the logarithm of Z is evaluated by replacing it by the logarithm of its maximum term (cf., e.g., Ref. 21). Maximizing the body of the sum in Eq. (3) with respect to the two degrees of freedom s_b and n_b, obeying Eq. (2), leads to two equations fully determining the local H coverages on the NM and fcc phase $\Theta_{H,NM}=n_b/s_b$ and $\Theta_{H,fcc}=n_f/(2s_f)$, respectively,

$$\frac{\Theta_{H,NM}}{2\Theta_{H,fcc}} = \frac{1-\Theta_{H,NM}}{1-2\Theta_{H,fcc}} e^{-\Delta E_A/k_B T}, \tag{4}$$

$$\frac{1-\Theta_{H,NM}}{(1-2\Theta_{H,fcc})^{1/2}} = e^{-d\Delta F^{fcc\rightarrow NM}/k_B T}. \tag{5}$$

The first equation is the well-known Langmuir-McLean segregation isotherm. The second results from the freedom of the NM phase to change its size. Since Eqs. (4) and (5) are valid independent of the total H coverage Θ_H, an increase in

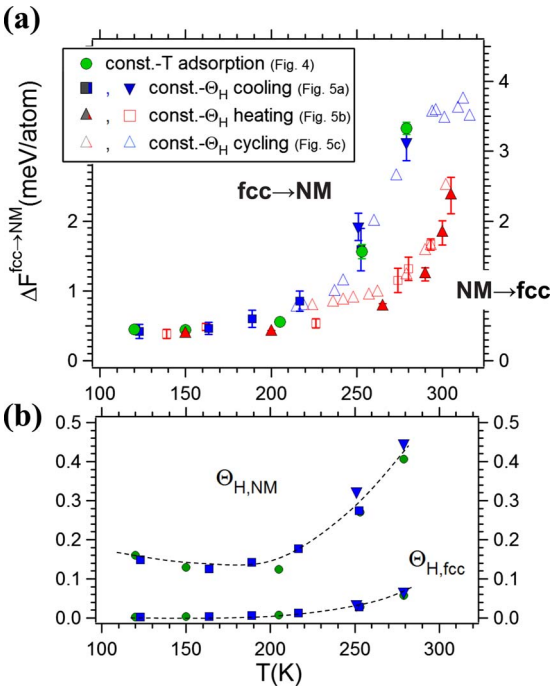

FIG. 7. (Color online) (a) Free-energy difference $\Delta F^{\mathrm{fcc}\rightarrow\mathrm{NM}}(T)$ for 4 ML films calculated from the $f_{\mathrm{NM}}(T,D)$ values measured at constant-temperature (const.-T, Fig. 4) and (near) constant coverage (const.-Θ_{H}, symbols as in Fig. 5). Note that the energy scale carries an uncertainty of a factor of 2 (cf. text). (b) Corresponding calculated local H coverages on the NM and fcc phases shown for the forward fcc→NM transition only. The lines are guides to the eye.

Θ_{H} leads to an increase in the NM fraction $f_{\mathrm{NM}}=s_{\mathrm{b}}/s$ according to

$$\Theta_{\mathrm{H}} = f_{\mathrm{NM}}\Theta_{\mathrm{H,NM}} + (1-f_{\mathrm{NM}})\Theta_{\mathrm{H,fcc}}. \tag{6}$$

Since Θ_{H} cannot be measured directly, it is estimated by a second-order adsorption law

$$\Theta_{\mathrm{H}}(D) = \frac{DS_0R}{1+DS_0R} \tag{7}$$

for dissociative adsorption of H_2 molecules with an initial sticking probability of $S_0 \approx 0.1$ approximately known from 6 ML Fe/Cu(100) experiments.[15] This is six to eight times higher than on low index bcc Fe surfaces[22] and slightly smaller than on the Fe/Rh(100) ultrathin film system (0.1–0.3),[23] which contains Fe in a tetragonal state between fcc and bcc.[24] $R=1.87$ ML/L is a constant factor for 300 K H_2-gas temperature. The correct adsorption law, taking into account different local H coverages on the two phases, deviates only little (<10%) from Eq. (7) for the rather low coverages in the experiments.

Equations (4)–(7) are then used to fit the uptake curves $f_{\mathrm{NM}}(D)$ (Fig. 4) with one parameter $\Delta F^{\mathrm{fcc}\rightarrow\mathrm{NM}}(T)$ for each curve and a common, i.e., temperature-independent parameter ΔE_{A} mainly determined by the onset delays in the $f_{\mathrm{NM}}(D)$ curves above 200 K. The resulting ΔE_{A} of ≈ −40 meV is consistent with thermal-desorption spectroscopy experiments by Egawa *et al.*[25] showing two H_2 desorption peaks separated by only 15–30 K. The same ΔE_{A} is used to directly calculate $\Delta F^{\mathrm{fcc}\rightarrow\mathrm{NM}}(T)$ values from each of the $f_{\mathrm{NM}}(T,D)$ values of the (near) constant-coverage experiments (Fig. 5), accounting for the actual dose including background-H_2 adsorption. For the two experiments, where the exact initial dose is not known (open symbols in Figs. 5 and 7), the initial dose is treated as an additional fit parameter, and is determined by matching the resulting $\Delta F^{\mathrm{fcc}\rightarrow\mathrm{NM}}(T)$ curves to those from experiments with known initial doses (closed symbols).

Eventually all experimental $f_{\mathrm{NM}}(T,D)$ values collapse onto one $\Delta F^{\mathrm{fcc}\rightarrow\mathrm{NM}}(T)$ curve (Fig. 7), which reflects the tendency already present in the raw data, i.e., no significant change below 200 K, and a distinct temperature dependence above. Evidently, the assumption that the system can reach its thermal equilibrium is not exactly fulfilled, and the equilibrium values have to be estimated by averaging heating and cooling curves. Such a hysteresis is not unusual for phase transitions in Fe, although it is much smaller than in fcc-bcc transitions in bulk Fe alloy systems, where it is rather of the order of hundreds of kelvin.[26] The corresponding temperature dependence of $\Theta_{\mathrm{H,NM}}$ [Fig. 7(b)] is similar but less strong than that of $\Delta F^{\mathrm{fcc}\rightarrow\mathrm{NM}}$ since not only the total number of H atoms, but also their configuration entropy determines the NM fraction that can form.

This quantification procedure, however, carries a scale uncertainty as the uncertainty of the actual H coverage, mainly determined by the uncertainty of the product DS_0 in Eq. (7), adds up to a factor of two (both in direction of larger and smaller values). Additional uncertainties due to the approximations in Eq. (1) may be assessed by comparison with calculations of the similar H/Fe(110) system by Jiang and Carter[27] and Cremaschi *et al.*:[28] (1) the splitting of the total energy ε into two terms in Eq. (1), i.e., the separability of H surface chemistry and Fe "bulk" physics, is strictly valid only if the electronic structure of the film is not influenced too much by the presence of the H atoms on the surface, i.e., if the film thickness is high and the surface coverage low. The bonding of H to the surface Fe(110) atoms is "quite covalent, involving primarily… Fe 4*sp* electrons"[27] with a rather small charge transfer of the order of 0.1 electrons. Even at $\Theta_{\mathrm{H}}=1$, the near Fermi-surface *d*-electron band structure and the surface exchange splitting is not dramatically changed.[27] Since the H coverage on the NM surface is in the range of 0.15–0.45 and the deeper Fe layers unaffected, the overall influence of the adsorbed H on the film except that of local bonding should therefore be negligible. (2) With the exception of site competition, the H atoms are assumed to be noninteracting. In the H/Fe(110) calculation,[27] repulsion of about 23 meV/H atom is found only for $\Theta_{\mathrm{H}}=1$, while it is negligible for $\Theta_{\mathrm{H}}=0.5$ in ordered H adsorption structures. In addition, the experimental ΔE_{A} effectively includes repulsion at least on average. (3) Vibrational contributions to the partition function [Eq. (3)], which may be included as entropy terms in ΔE_{A}, i.e., as a temperature dependence of ΔE_{A}, are neglected. This is acceptable since, in particular in the presence of H, the fcc Fe phase reconstructs, forming adsorption sites on the fcc phase that differ very little from those on the NM phase[15] (cf. Fig. 6). In the H/Fe(110) system, the stretch vibration frequencies of threefold-hollow-

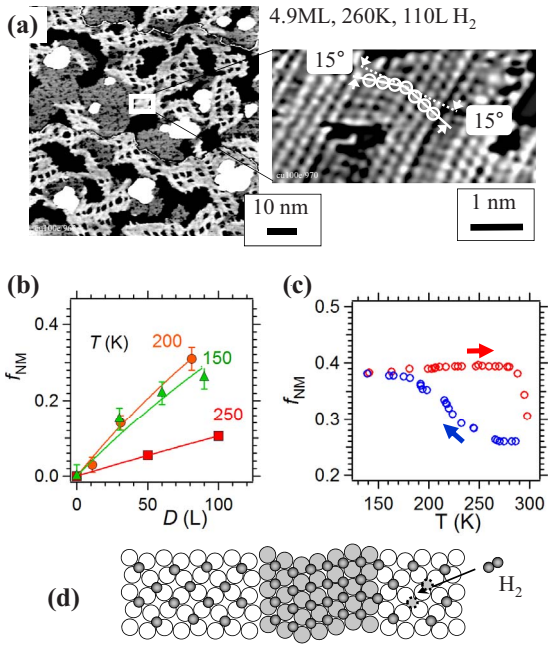

FIG. 8. (Color online) 5 ML films after exposure to large H_2 doses. (a) Overview and atomically resolved STM images of a film grown at 300 K, adsorption of 110 L H_2 at 200 K, and reheating to 260 K (−1 V, 0.1 nA and −1 mV, 5 nA, respectively). The local shear angle of 15° is indicated. The period of the NM reconstruction is about six to seven atom rows. (b) NM fraction in dependence of H_2 dose for three different temperatures. (c) NM fraction during a temperature cycle starting just below 290 K. (d) Schematic top view of H_2 adsorption at near saturation H coverage (≈0.5 on fcc, ≈1 on NM phase).

and bridge-type adsorption sites differ only by about 1%.[27,28] Modeling the adsorbed H atom as a three-dimensional harmonic oscillator to get an impression what effect a 1% difference of vibrational frequencies would have on ΔE_A in the considered 100–300 K temperature interval results in only about 0.1 meV per 100 K, which shows that the temperature dependence of ΔE_A cannot be very important.

D. 5 ML films

Five ML films do not form a NM phase even in the H contaminated as-grown form. However, it does form after exposure to high H_2 doses, i.e., with a nearly H saturated film surface (Fig. 8). The H_2 doses needed for a certain NM fraction f_{NM} may change substantially depending on the density of monatomic holes (exact film thickness), annealing procedure, and history of thermal cycling of the already H covered film, e.g., annealed films require even higher doses to form the NM phase. Therefore only data from as-grown films with 4.9 ± 0.1 ML thickness are shown in Fig. 8(b). This indicates that the NM phase in 5 ML films is close to the point where even saturation H coverage can no longer stabilize the NM phase. This correlates again strongly with the magneto-optical Kerr effect measurements by Vollmer and Kirschner,[11] which show that the films can be made fully ferromagnetic up to 5 ML thickness by growth in a H_2 atmosphere of about 10^{-7} mbar.

The high H_2 doses D necessary and the rather linear increase in the NM fraction with D can be understood in terms of second-order adsorption on a nearly H saturated surface, i.e., if the effective sticking coefficient is proportional to the very low number of H-vacancy pairs on the fcc surface as sketched in Fig. 8(d). As in the 4 ML system, the growing NM phase with its higher capacity for H atoms will remove H atoms from the fcc regions, leaving $\Theta_{H,fcc}$ and the number of adsorption sites proportional to $(1/2-\Theta_{H,fcc})^2$ almost constant.

Appearance of the 5-ML NM phase [Fig. 8(a)] and qualitative temperature dependence [Figs. 8(b) and 8(c)] are almost exactly the same as for the 4 ML films. The experiment in Fig. 8(c) is similar to the temperature cycle experiment with 4 ML films, i.e., initially the sample was held at a temperature where the NM fraction decreases slowly due to H_2 desorption before cooling the sample at a rate of 1–3 K/min. Below 270 K the NM fraction increased but became again almost temperature independent below ≈200 K. On heating there was little change until 280 K where the NM phase started to disappear due to H_2 desorption rather abruptly, about 30 K earlier compared to 4 ML films. This is related to the fact that the temperature where efficient H_2 desorption starts is distinctly lower in 5 ML films because the second-order H_2 desorption rate (proportional to $\Theta^2_{H,fcc}$) is 25–100 times higher in 5 ML films than in 4 ML films due to the 5–10 times higher H coverage on the NM and fcc surface, respectively. Nevertheless, the hysteresis of the reversible transition seems to be larger than in 4 ML films. The decrease in f_{NM} due to an increase in $\Delta F^{fcc\rightarrow NM}$ as in 4 ML films seems not to be observable in 5 ML films.

Exact quantitative evaluation such as that done for the 4 ML films is not easily possible for various reasons, some of them mentioned above. An estimate for $\Delta F^{fcc\rightarrow NM}$, however, can be obtained from the observation that full H coverage $(n_b/s_b \approx 1)$ is just enough to tip the balance from fcc to NM, i.e., $\varepsilon \approx 0$ in Eq. (1), resulting in $\Delta F^{fcc\rightarrow NM} \approx -\Delta E_A/d = 8$ meV per atom.

IV. DISCUSSION

This section serves to consolidate the thickness and temperature-dependent experimental results acknowledging that there should be an increasing correspondence to bulk Fe with increasing film thickness. A semiquantitative theory of the phase stability in bulk Fe has been proposed by Hasegawa and Pettifor,[9] which is based entirely on magnetic contributions to the free-energy difference between the phases, neglecting vibrational contributions. The theory of Fe magnetism[29,30] used in this model attempts to reconcile the band theory of itinerant magnetism with the presence of magnetic on-site correlation, which naturally leads to two types of magnetic ordering: (1) the formation of average "local" magnetic moments (on-site correlation) (2) whose direction varies from site to site for $T>0$ (long-range ordering). The magnetic moment itself stabilizes the bcc phase (cf., e.g., Ref. 31) and is essentially temperature independent because of the large exchange splitting of the order of 1 eV or 10 000 K.[29] The energy gained by long-range magnetic or-

dering of the local moments is one magnitude smaller and the related entropy difference between the disordered fcc and the ordered bcc phase describes the temperature dependence in the Fe phase diagram[9] (cf. Sec. IV B).

Both aspects of the magnetic structure may be modified in nanoscale systems. For instance, changes in the temperature-independent phase stability may indicate surface modified (local) magnetic moments while changes in the temperature-dependent stability may be caused by surface modified long-range magnetic order. In the following subsections possible manifestations of this close relationship between magnetism and structure in the thickness and temperature-dependent film stability are pointed out.

A. Thickness dependence

In order to see to what extent ultrathin films correspond to or differ from bulk Fe, the groundstate energy difference between bulk Fe and ultrathin Fe films, $E_{\mathrm{film}}(d)-E_{\mathrm{bulk}}$, may be partitioned into a deformation energy E_D, necessary to convert the respective bulk structure (bcc or fcc) into its usually strained ultrathin film version, and a thickness dependent term γ/d with a combined surface-interface energy γ accounting for all finite-thickness effects,

$$E_{\mathrm{film}}(d) = E_{\mathrm{bulk}} + E_D + \gamma/d. \tag{8}$$

In the following, γ is assumed to be thickness independent, which is exact only in absence of surface-interface interaction, and the d^{-1} dependence represents the increasing weight of the surface and interface energies with decreasing thickness. However, if surface and interface interact, γ can depend on thickness and should therefore be considered with caution when used for the description of films less than 5 ML thick.[32]

For the phase stability only energy differences to the fcc phase are relevant; in particular the known ground-state energy difference of bulk Fe $\Delta E_{\mathrm{bulk}}^{\mathrm{fcc}\to\mathrm{bcc}} \approx 50-57$ meV/atom,[2,33] the relative deformation energy $\Delta E_D^{\mathrm{fcc}\to\mathrm{X}} = E_D^{\mathrm{X}} - E_D^{\mathrm{fcc}}$, and the relative surface-interface energy $\Delta\gamma^{\mathrm{fcc}\to\mathrm{X}} = \gamma^{\mathrm{X}} - \gamma^{\mathrm{fcc}}$ for X=bcc or NM. Interlayer distances from a multiple-scattering low-energy electron-diffraction (Tensor-LEED-I/V) analysis of 6 ML fcc films[4] indicate that the structures of bulk fcc Fe and the "bulk" of pseudomorphic fcc films are essentially identical (estimated strain energy in fcc films ≈ 1 meV/atom) and therefore $E_D^{\mathrm{fcc}} \approx 0$ is assumed.

In Fe films with the ideal bcc structure, E_D^{bcc} is zero by definition, and $\Delta\gamma^{\mathrm{fcc}\to\mathrm{bcc}}$ mainly determined by the substantial lattice mismatch between fcc(100) Cu and bcc(110) Fe, i.e., the total film energy

$$\Delta E_{\mathrm{film}}^{\mathrm{fcc}\to\mathrm{bcc}} = \Delta E_{\mathrm{bulk}}^{\mathrm{fcc}\to\mathrm{bcc}} + \Delta\gamma^{\mathrm{fcc}\to\mathrm{bcc}}/d \tag{9}$$

must become *larger* with decreasing thickness [Fig. 9(a)]. Below a certain critical thickness, fcc films are more stable. Clean bcc films on Cu(100) form spontaneously above about 11 ML thickness,[3,7] but since it is possible to trigger the transition to the relaxed bcc phase by ion bombardment already in 8 ML fcc films,[10] this limit is probably closer to 6 ML thickness, although this is an educated guess only.

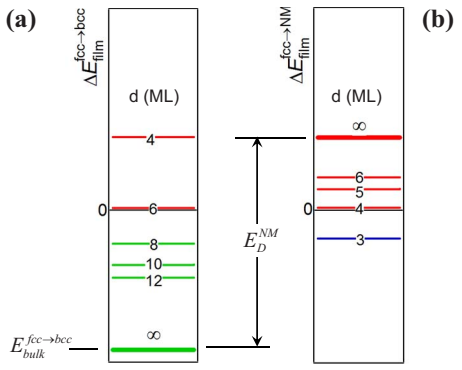

FIG. 9. (Color online) Illustration of the estimated bcc and NM ground-state energies relative to the fcc phase in dependence of thickness d. Positive values indicate a stable fcc phase. (a) Films with bcc structure: The finite-thickness correction $\Delta\gamma^{\mathrm{fcc}\to\mathrm{bcc}}/d$ to the bulk value $\Delta E_{\mathrm{bulk}}^{\mathrm{fcc}\to\mathrm{bcc}}$ is positive due to the interface lattice mismatch, which stabilizes the fcc phase below a critical thickness, which is assumed to be around 6 ML (cf. text). (b) Films with the NM structure are stable because the sequence of stability in dependence of film thickness is reversed, i.e., the finite-thickness correction $\Delta\gamma^{\mathrm{fcc}\to\mathrm{NM}}/d$ is negative, stabilizing the NM phase for $d \lesssim 4$. The values for bulk Fe and a fictitious, infinitely thick NM film are separated by the deformation energy E_D^{NM}.

In NM films the deformation term E_D^{NM} is certainly important as the NM phase is strongly strained and contains a high density of twin boundaries. Most remarkably, the experimental results in the previous sections show that the groundstate energy difference

$$\Delta E_{\mathrm{film}}^{\mathrm{fcc}\to\mathrm{NM}} = \Delta E_{\mathrm{bulk}}^{\mathrm{fcc}\to\mathrm{bcc}} + E_D^{\mathrm{NM}} + \Delta\gamma^{\mathrm{fcc}\to\mathrm{NM}}/d \tag{10}$$

becomes *smaller* with decreasing thickness. In particular, $\Delta E_{\mathrm{film}}^{\mathrm{fcc}\to\mathrm{NM}}(3)$ must be negative, since in 3 ML films the NM phase is more stable than the fcc phase (Fig. 2). First-principles calculations[6] indicate that the NM phase is stable with respect to the FM fcc phase by 13 meV. If there exists an antiferromagnetic or spin-density wave structure that is more stable than the ferromagnetic fcc structure (but still less stable than the NM structure), $\Delta E_{\mathrm{film}}^{\mathrm{fcc}\to\mathrm{NM}}(3)$ would be somewhat above -13 meV. The experiments described here provide approximate numbers for the ground-state values $\Delta E_{\mathrm{film}}^{\mathrm{fcc}\to\mathrm{NM}}(4) \approx 0$ and $\Delta E_{\mathrm{film}}^{\mathrm{fcc}\to\mathrm{NM}}(5) \approx +8$ meV/atom. Moreover, it has been shown previously[15] that in 6 ML films only a (1×2) surface reconstruction can be induced by massive H_2 dosing, but no NM phase appears, i.e., the 6 ML groundstate value of the NM phase must be even larger than that of the 5 ML films. The sequence of ground-state energy differences matching these values is sketched in Fig. 9(b) for $\Delta\gamma^{\mathrm{fcc}\to\mathrm{NM}} \approx -150$ meV and $E_D^{\mathrm{NM}} \approx 85$ meV/atom. Since these values depend on the rather crude approximation for $\Delta E_{\mathrm{film}}^{\mathrm{fcc}\to\mathrm{NM}}(5)$ and the assumption that $\Delta\gamma^{\mathrm{fcc}\to\mathrm{NM}}$ is thickness independent, they cannot be very precise either but are nevertheless useful to test whether the model of a deformed bcc phase is reasonable or not.

For this purpose, the deformation energy E_D^{NM} is compared to the sum of elastic strain and twin boundary energies. Twin boundary energies in Fe are generally very small; of

the order of 5 meV per boundary atom[34] or one third of this value on average per film atom for the NM structure shown in Fig. 1. If the density of boundaries is as high as in the NM phase, the value maybe much higher (twin boundary repulsion[16]), but even then it can only be a smaller fraction of the total deformation energy. Therefore the estimated $E_D^{\mathrm{NM}} \approx 85$ meV/atom should be only a little larger than the strain energy necessary to change the bcc structure to the local NM structure: An expansion of the strain energy to second and third order using experimental elastic constants of bcc Fe, which under- or overestimate the true value, respectively, limits the possible range to 40–80 meV.[12] First-principles[31] and semiempirical[35] results for the bct unit cell approximating the NM unit cell best (lattice-parameter ratio $c/a=1.15$) are 60 and 70 meV/atom, respectively. Accepting 60 meV/atom as a likely value for the elastic strain energy, the remaining 25 meV/atom for the twin boundary energy, complementing $E_D^{\mathrm{NM}} \approx 85$ meV, is very high, but given the abovementioned uncertainties, the agreement is acceptable for the purpose to demonstrate the consistency of the description of the NM phase as a deformed bcc phase.

The negative sign of the total surface-interface term $\Delta\gamma^{\mathrm{fcc}\rightarrow\mathrm{NM}}$ implies the presence of a negative surface-interface contribution that is in absolute numbers larger than the certainly positive fcc-NM lattice mismatch term, although the latter should not be very large given the equal interface atom density and the absence of unfavorable on-top atom stacking situations. It has been shown in a detailed first-principles analysis of the 3*d* transition-metal surfaces[36] that the surface energies are substantially lowered due to magnetism in particular for Cr, Mn, Fe, and Co surfaces accompanied by enhanced surface magnetic moments. Given the large surface magnetic moments suggested by spin-polarized appearance potential spectroscopy,[37] which are even larger than those of the bcc(110) surface, it is plausible that the bcc-like NM phase could have a lower surface energy than the (surface reconstructed) fcc surface, providing a possible explanation for the negative $\Delta\gamma^{\mathrm{fcc}\rightarrow\mathrm{NM}}$.

Another finite-thickness contribution to the relative stability of the NM phase may arise if the fcc phase becomes less stable with decreasing thickness: As shown by Asada and Blügel,[38] the increasing difficulty (frustration) to realize a magnetically compensated (every spin-up has a spin-down partner) bilayer-antiferromagnetic structure "*AABB*" in ultrathin fcc Fe films, e.g., with an uneven number of layers *d* or $d<4$, may destabilize the fcc phase at low thicknesses and therefore may also increase the relative stability of the NM phase in the thickness region below 6 ML thickness.

B. Temperature dependence

In the Hasegawa-Pettifor model of Fe phase stability,[9] the slope of the $\Delta F^{\mathrm{fcc}\rightarrow\mathrm{bcc}}(T)$ curve is related to the magnetic entropy difference $\Delta S^{\mathrm{fcc}\rightarrow\mathrm{bcc}}$ between the phases according to $S=-dF/dT$ at zero pressure. If both phases are magnetically ordered or both are disordered, e.g., Fe above its Curie temperature, $\Delta S^{\mathrm{fcc}\rightarrow\mathrm{bcc}}$ is small and $\Delta F^{\mathrm{fcc}\rightarrow\mathrm{bcc}}$ therefore near constant. In the simplified "minimum model" shown in Fig. 10(b) it is further assumed that at the critical temperatures

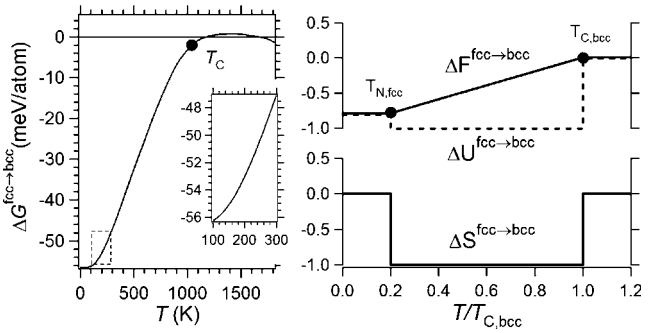

FIG. 10. Illustrations to the temperature-dependent phase stability in Fe. (a) Gibbs free-energy difference of bulk Fe at 1 atm by Kaufman, Clougherty, and Weiss.[2] The inset shows the curve enlarged in the temperature region between 130 and 300 K with the same axis ratio as in Fig. 7 to facilitate direct comparison. (b) Simplified dependence of (normalized) entropy, internal energy, and free-energy differences ΔS, ΔU, and ΔF if phase stability is determined only by magnetic contributions.

the magnetic order parameter jumps abruptly from minimum to maximum value and that the basic relation $F=U-TS$ holds. This linearized picture approximates the experimental free-energy difference between the fcc and bcc phases[2] of bulk Fe around $T_{\mathrm{C,bcc}}$ depicted in Fig. 10(a) quite well. Note that the difference between Helmholtz and Gibbs free energies $\Delta F^{\mathrm{fcc}\rightarrow\mathrm{bcc}}$ and $\Delta G^{\mathrm{fcc}\rightarrow\mathrm{bcc}}$, respectively, at atmospheric pressure is negligibly small.

The inset in Fig. 10(a) shows a change of the bulk free-energy difference $\Delta G^{\mathrm{fcc}\rightarrow\mathrm{bcc}}$ by about 9 meV per atom between 130 and 300 K, i.e., a slope of the order of 50 μeV/K per atom in the region where the fcc phase is magnetically disordered and the bcc phase ordered. If ultrathin films behave thermodynamically like bulk Fe, a similar temperature dependence of the stability of the NM phase relative to the fcc phase may be expected. The experimental results depicted in Fig. 7(a) show that this hypothesis can only partly be confirmed by experiment. While in 4 ML films above 200 K the slope in fact is of the order of 50 μeV/K (with an uncertainty of a factor of 2, cf. Sec. III C), the slope decreases rapidly below 200 K, which has the consequence that well annealed 4 ML films free of H cannot be converted to the NM phase even at 130 K.

Generally, ultrathin films differ from bulk Fe by their critical temperatures, which in the most simple picture of bulk-terminated thin films should be lower due to the lack of exchange partners at their surfaces.[39] The fcc surface, however, is reconstructed forming local bcc-like configurations[15] (cf. Fig. 6) and is ferromagnetic[37] up to a remarkably high Curie temperature of $T_{\mathrm{C,fcc}}(\mathrm{s}) \approx 250-280$ K.[3,11,40] Deeper layers show antiferromagnetic or spin-density wave order[6,38,40] up to a Néel temperature of $T_{\mathrm{N,fcc}} \approx 200$ K.[3,40] Since bulk fcc Fe shows antiferromagnetic tendencies only at $\approx$60 K (Ref. 41) it must be the ferromagnetic surface and possibly also the Fe-Cu interface that stabilize magnetic order in the deeper layers of the ultrathin fcc Fe films.[42] Since the H stabilized 4-ML NM phase is ferromagnetic at least up to $\approx$300 K in ultrahigh vacuum and even up to $\approx$350 K provided sufficient high H_2 partial pressure,[11] below

$\approx$200 K both fcc and NM phase show magnetic long-range order and the magnetic entropy difference between the phases becomes very small. If the total entropy is dominated by magnetic entropy as suggested by Hasegawa and Pettifor,[9] the free-energy difference $\Delta F^{\mathrm{fcc}\rightarrow\mathrm{NM}}$ must become temperature independent below 200 K as illustrated in Fig. 10(b) and experimentally observed in the 4 ML and 5 ML films (Figs. 7 and 8).

Finally the temperature dependence of 3 ML films is briefly discussed; in particular the observed reduction of the shear angle around 300 K (cf. Sec. III A). These films are special as they are the thickest films forming the NM phase spontaneously without the help of H_2 and the thinnest films which may still be considered as relatively undisturbed by Cu due to interface intermixing.[12,43] A combination of the thickness and temperature dependence in Figs. 9(b) and 10(b), respectively, for $T_{\mathrm{N,fcc}} \gtrsim 200$ K suggests the possibility of a NM-fcc phase transition around 400 K, which is right at the limit of thermal destruction of the films due to Cu diffusion to the film surface[18] and therefore difficult to access. At least up to 340 K no separate fcc phase has been seen in this work; only NM regions with a lower shear angle (cf. Fig. 2), suggesting the possibility of a more continuous NM$\rightarrow$fcc phase transition with a gradual decrease in the shear angle starting near rotational domain boundaries. On the other hand, the H induced transition in 4 ML films is clearly first order with separate fcc and NM regions. However, to be able to answer this question with confidence, detailed knowledge of the shape of the fcc-NM transition path is necessary, which may be additionally modified by intermixed Cu and surface H. For instance, first-principles calculations[6] suggest that 3 ML films differ from 4 ML films insofar as the 3-ML structure with the lowest energy, restricted to fcc symmetry, is ferromagnetic. The general instability of these solutions[6,35] (energy maximum) would paradoxically imply that there is no barrier between NM and fcc phase, rendering easier enforced deformations of the NM phase toward the fcc phase as they occur in the vicinity of rotational domain boundaries in 3 ML films [cf. Fig. 2(b)].

V. SUMMARY

The experiments presented provide detailed information on the thickness, temperature, and H coverage dependent stability of the bcc-like NM phase in 3–5 ML Fe films grown layer by layer on Cu(100) at 300 K. Three ML films are fully NM at least up to 340 K, although deviations from the ideal NM structure (smaller shear angle on average) are visible at this temperature. Clean, annealed 4 ML films are fcc in the entire temperature range considered (130–340 K), but a near reversible first-order transition to the NM phase occurs at rather low H coverage. Five ML films become NM at very high H_2 doses, i.e., near saturation H coverage. To obtain a more quantitative picture, the amount of H on the Fe film surface needed to stabilize the NM phase is used to estimate the free-energy difference $\Delta F^{\mathrm{fcc}\rightarrow\mathrm{NM}}(T)$ using a statistical mechanical description of the temperature-dependent interaction between surface H bonding and Fe film phase transition.

Empirically, the thickness dependent phase stability is described by separating $\Delta F^{\mathrm{fcc}\rightarrow\mathrm{bcc}}(T)$ or $\Delta F^{\mathrm{fcc}\rightarrow\mathrm{NM}}(T)$ into a bulk and a finite-thickness term. For the relative stability of bcc films, this finite-thickness term is dominated by the lattice mismatch between fcc(100) substrate and bcc(110) film and therefore positive, i.e., fcc stabilizing. NM films are also bcc-like but match the fcc(100) substrate much better. Therefore, as the continuous increase in the stability of the NM phase with decreasing thickness shows, lattice mismatch can only be a minor contribution to the finite-thickness energy in this case, which is now dominated by intrinsic (not substrate related), negative terms stabilizing the NM phase. Their origin may be either a lower surface energy of the NM structure due to enhanced surface magnetism[36,37] and/or a higher energy of the fcc phase due to frustration effects of the layerwise antiferromagnetic (or spin-density wave) order in very thin fcc films (<6 ML).[38] The curious sequence of stability of bcc(110), fcc(100), and bcc-like NM phases with decreasing film thickness is then explained as the successive operation of two finite-thickness effects of different strength, first film-substrate lattice mismatch stabilizing the fcc phase below 11 ML, second the weaker intrinsic finite-thickness terms stabilizing the NM phase below 5 ML thickness.

Furthermore it is found that the NM phase becomes more stable by lowering the temperature, similar to bulk bcc Fe. However, this is true only above 200 K while no significant further increase in the NM stability can be seen on cooling below 200 K in 4 and 5 ML films. This effect is correlated with the high critical temperatures in (surface reconstructed) ultrathin fcc Fe films of 200 K (Néel temperature) and 250–280 K (surface Curie temperature).[3,42] Such a correlation of long-range magnetic order and phase stability is required by theories[9] of Fe phase stability, which are based mainly on the magnetic free energy, i.e, if both fcc and NM phase show long-range magnetic order, irrespective of the type of order, the magnetic entropy difference and by that the temperature dependence of the phase stability must become very small.

These results demonstrate that the stability of the NM phase is characterized by significant intrinsic finite-thickness effects while some correspondence to bulk bcc Fe remains even in films less than 5 ML thick. Although ultrathin films are probably the only systems which are simple enough to sort out these phenomena, they should nevertheless be relevant also for more complex finite Fe systems such as free nanoparticles.[44]

ACKNOWLEDGMENTS

I gratefully acknowledge discussions with M. Schmid as well as his technical expertise. Helpful discussions with T. Waitz are also acknowledged.

[1] J. Cui, T. Shield, and R. James, Acta Mater. **52**, 35 (2004).
[2] L. Kaufman, E. V. Clougherty, and R. J. Weiss, Acta Metall. **11**, 323 (1963).
[3] D. Li, M. Freitag, J. Pearson, Z. Q. Qiu, and S. D. Bader, Phys. Rev. Lett. **72**, 3112 (1994).
[4] K. Heinz, S. Müller, and P. Bayer, Surf. Sci. **352-354**, 942 (1996).
[5] A. Biedermann, R. Tscheließnig, M. Schmid, and P. Varga, Phys. Rev. Lett. **87**, 086103 (2001).
[6] D. Spišák and J. Hafner, Phys. Rev. Lett. **88**, 056101 (2002).
[7] J. Thomassen, F. May, B. Feldmann, M. Wuttig, and H. Ibach, Phys. Rev. Lett. **69**, 3831 (1992).
[8] H. C. Herper, E. Hoffmann, and P. Entel, Phys. Rev. B **60**, 3839 (1999).
[9] H. Hasegawa and D. G. Pettifor, Phys. Rev. Lett. **50**, 130 (1983).
[10] W. Rupp, A. Biedermann, B. Kamenik, R. Ritter, C. Klein, E. Platzgummer, M. Schmid, and P. Varga, Appl. Phys. Lett. **93**, 063102 (2008).
[11] R. Vollmer and J. Kirschner, Phys. Rev. B **61**, 4146 (2000).
[12] A. Biedermann, R. Tscheliessnig, M. Schmid, and P. Varga, Appl. Phys. A: Mater. Sci. Process. **78**, 807 (2004).
[13] M. Zharnikov, A. Dittschar, W. Kuch, C. M. Schneider, and J. Kirschner, J. Magn. Magn. Mater. **174**, 40 (1997).
[14] A. Biedermann, M. Schmid, and P. Varga, Phys. Rev. Lett. **86**, 464 (2001).
[15] A. Biedermann, R. Tscheließnig, C. Klein, M. Schmid, and P. Varga, Surf. Sci. **563**, 110 (2004).
[16] A. G. Khachaturyan, S. M. Shapiro, and S. Semenovskaya, Phys. Rev. B **43**, 10832 (1991).
[17] M. Zharnikov, A. Dittschar, W. Kuch, C. M. Schneider, and J. Kirschner, Phys. Rev. Lett. **76**, 4620 (1996).
[18] J. Shen, J. Giergiel, A. K. Schmidt, and J. Kirschner, Surf. Sci. **328**, 32 (1995).
[19] T. Detzel and N. Memmel, Phys. Rev. B **49**, 5599 (1994).
[20] D. McLean, *Grain Boundaries in Metals* (Oxford University Press, Oxford, 1957).
[21] M. C. Flowers, N. B. H. Jonathan, A. Morris, and S. Wright, J. Chem. Phys. **108**, 3342 (1998).
[22] H. F. Berger and K. D. Rendulic, Surf. Sci. **251-252**, 882 (1991).
[23] C. Egawa, S. Oki, and Y. Murata, Surf. Sci. **304**, L488 (1994).
[24] D. Spišák and J. Hafner, Phys. Rev. B **73**, 155428 (2006).
[25] C. Egawa, E. M. McCash, and R. F. Willis, Surf. Sci. **215**, L271 (1989).
[26] L. Delaey, in *Phase Transformations in Materials*, edited by G. Kostorz (Wiley-VCH Verlag GmbH, Weinheim, 2001), p. 585.
[27] D. Jiang and E. A. Carter, Surf. Sci. **547**, 85 (2003).
[28] P. Cremaschi, H. Yang, and J. L. Whitten, Surf. Sci. **330**, 255 (1995).
[29] J. Hubbard, Phys. Rev. B **19**, 2626 (1979).
[30] N. M. Rosengaard and B. Johansson, Phys. Rev. B **55**, 14975 (1997).
[31] E. G. Moroni, G. Kresse, J. Hafner, and J. Furthmüller, Phys. Rev. B **56**, 15629 (1997).
[32] C. Friesen, Surf. Sci. **600**, 1012 (2006).
[33] W. Bendick and W. Pepperhoff, Acta Metall. **30**, 679 (1982).
[34] C. M. Wayman and H. K. D. H. Bhadeshia, in *Physical Metallurgy*, 4th ed., edited by R. W. Cahn and P. Haasen (North-Holland, Amsterdam, 1996), Vol. 2, p. 1507.
[35] G. L. Krasko and G. B. Olson, Phys. Rev. B **40**, 11536 (1989).
[36] M. Aldén, H. L. Skriver, S. Mirbt, and B. Johansson, Surf. Sci. **315**, 157 (1994).
[37] T. Detzel, M. Vonbank, M. Donath, and V. Dose, J. Magn. Magn. Mater. **147**, L1 (1995).
[38] T. Asada and S. Blügel, Phys. Rev. Lett. **79**, 507 (1997).
[39] G. A. T. Allan, Phys. Rev. B **1**, 352 (1970).
[40] D. Qian, X. F. Jin, J. Barthel, M. Klaua, and J. Kirschner, Phys. Rev. Lett. **87**, 227204 (2001).
[41] U. Gonser, C. J. Meecham, A. H. Muir, and H. Wiedersich, J. Appl. Phys. **34**, 2373 (1963).
[42] D. Qian, X. F. Jin, J. Barthel, M. Klaua, and J. Kirschner, Phys. Rev. B **66**, 172406 (2002).
[43] H. L. Meyerheim, R. Popescu, D. Sander, J. Kirschner, O. Robach, and S. Ferrer, Phys. Rev. B **71**, 035409 (2005).
[44] G. Rollmann, M. E. Gruner, A. Hucht, R. Meyer, P. Entel, M. L. Tiago, and J. R. Chelikowsky, Phys. Rev. Lett. **99**, 083402 (2007).